JOURNAL OF PROPULSION AND POWER
Vol. 13, No. 1, January–February 1997

Chordwise Bending Cascade Unsteady Aerodynamics by an Experimental Influence Coefficient Technique

Daniel A. Ehrlich* and Sanford Fleeter†
Purdue University, West Lafayette, Indiana 47907

The chordwise bending unsteady aerodynamics of an annular cascade of flat-plate airfoils are investigated utilizing an experimental influence coefficient technique. A single airfoil in the cascade is forced to oscillate in a chordwise bending mode over a range of reduced frequencies. Unsteady surface pressures induced on the oscillating airfoil and its stationary neighbors are measured to determine the unsteady aerodynamic influence coefficients. These influence coefficients are then summed vectorially to obtain unsteady airfoil surface loadings. The experimental data are correlated with predictions from linearized unsteady aerodynamic theory. The linearized analysis accurately predicts trends in both the influence coefficients and the unsteady airfoil surface loadings. The data show the cascade to be unstable at all values of the reduced frequency, whereas linearized theory predicts the cascade to be stable or only marginally unstable. The discrepancy between the data and prediction is attributed to the sensitivity of the aerodynamic work per cycle calculation to uncertainty in measured unsteady surface pressure difference phase in the airfoil midchord and leading-edge regions and to differences in measured and predicted unsteady surface pressure-difference magnitude near the leading edge of the airfoil.

Nomenclature

A_c = chordwise bending-mode-shape amplitude
C = airfoil chord
C_p = unsteady surface pressure coefficient
$\hat{C}_p^n$ = unsteady pressure influence coefficient induced by the oscillation of airfoil n
$h(x)$ = first harmonic normalized airfoil deflection
k = reduced frequency, $\omega C/U$
M = cascade inlet Mach number
$\tilde{P}$ = instantaneous airfoil surface static pressure
p_j = jth harmonic airfoil surface static pressure complex amplitude
$\tilde{p}_j$ = jth harmonic of unsteady airfoil surface static pressure
$\boldsymbol{R}$ = airfoil surface displacement relative to mean airfoil position
U = freestream velocity
W_c = unsteady aerodynamic work per cycle of airfoil motion
$\bar{W}_c$ = dimensionless unsteady aerodynamic work per cycle
w = airfoil surface upwash velocity
$\bar{w}$ = complex amplitude of airfoil surface upwash velocity
$\bar{w}_c$ = pressure-difference displacement function
x = dimensionless airfoil chordwise coordinate or percent chord
y = dimensionless coordinate normal to chordwise direction, Y/A_c
$\bar{y}$ = amplitude of airfoil surface displacement normal to chord
β = cascade interblade phase angle, positive when airfoil $n+1$ leads airfoil n
ΔC_p = unsteady pressure-difference coefficient
$\Delta \hat{C}_p^n$ = unsteady pressure-difference influence coefficient
ϕ_p = phase of unsteady pressure
ω = airfoil oscillation frequency

Subscripts
B = airfoil mean position
$\mathcal{B}$ = airfoil instantaneous position

Superscripts
l = airfoil lower surface
u = airfoil upper surface

Introduction

NEW technologies are being developed to achieve higher performance in advanced gas-turbine engines. In general, these also cause higher vibratory blade row responses and stresses. In particular, the design trend toward higher stage loadings and higher specific flow are being attained through increased tip speeds, higher through-flow and rotor relative Mach numbers, lower radius ratios, lower airfoil aspect ratios (ARs), and fewer stages. The resultant axial flow compressor blade designs utilize thin, low-AR blading with corresponding high steady-state stresses. Also, the mechanical damping is considerably reduced in newer rotor designs, particularly those with integral blade–disk configurations (blisks) and in those without shrouds. As a result, advanced axial flow blade designs feature low-AR blading that have significant unsteady flow-induced vibration problems, both flutter and forced response.

The unsteady aerodynamics associated with flutter are analyzed by considering a harmonic oscillating airfoil cascade to predict the motion-induced unsteady aerodynamics, i.e., the aerodynamic damping. With regard to forced response, the unsteady aerodynamic blade row response to a given forcing function is comprised of two components: 1) the gust response and 2) the motion-induced or aerodynamic damping. With mechanical damping considerably reduced in newer rotor designs, for example, blisks, the aerodynamic damping determines the level of response. Thus, for both flutter and flow-induced vibrations, it is important to investigate and quantify the motion-induced unsteady aerodynamics, the aerodynamic damping.

Critical turbomachine blade row flow-induced vibration modes are associated with the blade AR. High-AR blades resemble beams, with the resulting response typically occurring in the lower-order modes, i.e., simple bending and torsion. However, the vibration characteristics of low-AR blades more closely resemble plates than beams. As a result, for advanced

Received Oct. 28, 1994; revision received April 26, 1996; accepted for publication May 1, 1996. Copyright © 1996 by D. A. Ehrlich and S. Fleeter. Published by the American Institute of Aeronautics and Astronautics, Inc., with permission.

*Graduate Research Assistant, School of Mechanical Engineering.
†McAllister Distinguished Professor, School of Mechanical Engineering.

blade rows, chordwise bending modes of flow-induced vibration are significant. Chordwise bending unsteady aerodynamics research results are minimal or nonexistent. The primary emphasis to date has been directed at bending and torsion unsteady aerodynamics of importance to high-AR blading. To this end, a number of fundamental bending and torsion oscillating airfoil cascade experiments directed at quantifying the cascade aerodynamic damping have been performed.

The overall objective of this research is to investigate and quantify the chordwise bending-mode unsteady aerodynamics of an airfoil cascade in subsonic flow. Specific objectives include the development of an airfoil drive system to generate and control the airfoil chordwise bending-mode oscillations, the development and implementation of experimental techniques to determine airfoil surface chordwise bending-mode unsteady aerodynamics over the complete range of interblade phase angles, the acquisition and analysis of airfoil surface chordwise bending-mode unsteady aerodynamic data, and the correlation of these data with linear theory predictions.

Technical Approach

The unsteady aerodynamics of an airfoil cascade oscillating in a chordwise bending mode were experimentally investigated in the Purdue Annular Cascade Research Facility, thereby enabling the aerodynamic damping to be determined with a uniform inlet flow velocity over a range of reduced frequency values. A piezoelectric crystal-based airfoil drive system is developed and utilized to generate and control the airfoil chordwise bending-mode oscillations.

Oscillating airfoil cascade data are traditionally obtained by simultaneously oscillating all of the cascade airfoils at a constant interblade phase angle, with the unsteady airfoil surface pressures then measured. These experiments are extremely expensive, requiring the construction of complex drive systems to oscillate an entire cascade of airfoils at realistic reduced frequencies and a constant interblade phase angle. They are also time consuming because they must be performed over the complete interblade phase angle range.

The unsteady aerodynamic influence coefficient technique provides an alternative method for obtaining experimental oscillating cascade data. In this method, a single airfoil in the cascade is oscillated with the resulting unsteady pressure induced on this oscillating airfoil and its stationary neighbors measured. These unsteady pressures on the oscillating and stationary airfoils, expressed as pressure coefficients $\hat{C}_p^n(x)$, are the unsteady aerodynamic influence coefficients. The unsteady aerodynamics of a cascade having all airfoils oscillating at a specified, constant interblade phase angle are obtained through a vector summation of these unsteady aerodynamic influence coefficients.

Consider a two-dimensional, infinite cascade of flat-plate airfoils (Fig. 1), oscillating simultaneously with constant β. The unsteady pressure coefficient $C_p(x, \beta)$ at a point on the surface of a reference airfoil, Airfoil 0, is represented by a Fourier series summation of complex-valued unsteady aerodynamic influence coefficients

$$C_p(x, \beta) = \sum_{n=-\infty}^{+\infty} \hat{C}_p^n(x) e^{in\beta} \tag{1}$$

where the summation index n indicates that the influence coefficient $\hat{C}_p^n(x)$ represents the unsteady pressure coefficient induced on the reference airfoil by the oscillation of an airfoil at relative position n.

Equation (1) is used to calculate the unsteady loading on a typical airfoil in the cascade oscillating at an arbitrary constant interblade phase angle value once the unsteady aerodynamic influence coefficients are determined. The unsteady aerodynamic influence coefficients for a specified cascade configuration can be determined from the unsteady surface pressure distribution on a typical airfoil by inverting Eq. (1).

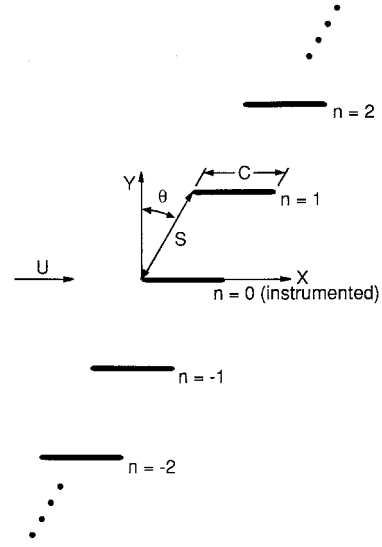

Fig. 1 Two-dimensional infinite cascade model.

$$\hat{C}_p^n(x) = \frac{1}{2\pi} \int_{-\pi}^{\pi} C_p(x, \beta) e^{-in\beta} \, d\beta \tag{2}$$

In this manner, unsteady airfoil loadings predicted by analytical oscillating cascade models can be used to calculate influence coefficients for comparison with experimental data.

Validation of the unsteady aerodynamic influence coefficient technique has been achieved by several researchers through comparison of influence coefficient results with data obtained from cascade experiments performed with all airfoils oscillating. Most recently, Kovats[1] showed favorable results for the comparison of predictions of aerodynamic damping and stability of low-pressure turbine blades. Buffum and Fleeter[2] also found good agreement between the influence coefficient method and all airfoils oscillating data for torsional flutter in a linear cascade at moderate subsonic Mach numbers. The results of Hanamura et al.[3] for experiments performed in a water channel also appear to validate the unsteady aerodynamic influence coefficient technique.

Experimental Facility

Purdue Annular Cascade Research Facility

The experiments were conducted in the Purdue Annular Cascade Research Facility, shown schematically in Fig. 2. The facility is an open-loop draw-through wind tunnel. A centrifugal fan located downstream of the test section and driven by a 224-kW (300-hp) induction motor draws air through the facility. This fan is capable of producing steady test-section velocities ranging from 6.4 m/s (20 ft/s) to 70 m/s (220 ft/s). Test-section velocity is fixed by throttling the fan using a damper located at the fan inlet.

The test section is configured with an isolated stator vane row of 36 flat-plate airfoils mounted at a stagger angle of 0 deg to achieve a zero mean incidence flow condition and eliminate steady loading effects. The flat-plate airfoils have a chord length of 17.78 cm (7.0 in.) and a span of 14.99 cm (5.9 in.), resulting in an airfoil AR of 0.85 and a cascade solidity of 1.83. Thirty-four of the stator vanes are uninstrumented, having a thickness of 0.48 cm (0.1875 in.). Of the two remaining cascade airfoils, one is a stationary aluminum airfoil instrumented along its midspan with a chordwise distribution of nine dynamic pressure transducers. To mount these transducers within the body of the flat-plate airfoil, it is necessary to increase the thickness of this airfoil to 0.96 cm (0.375 in.). The

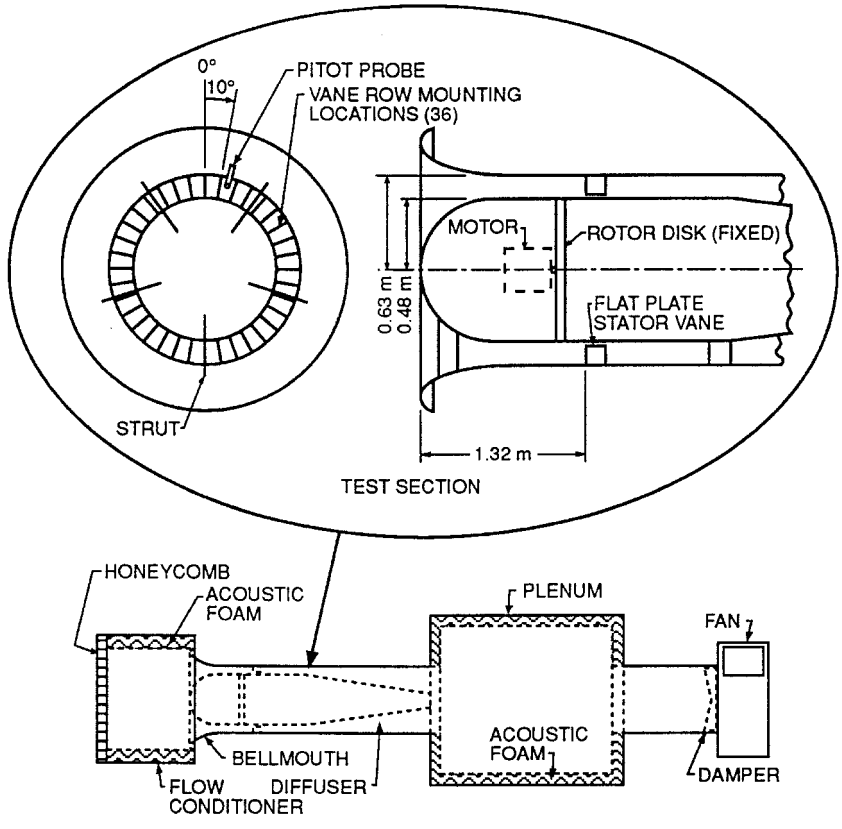

Fig. 2 Purdue annular cascade research facility.

final airfoil in the cascade is the chordwise bending-mode oscillating airfoil that is also instrumented at nine chordwise locations.

Chordwise Bending Oscillating Airfoil

The unsteady surface pressure influence coefficient distributions are produced by the two-dimensional chordwise bending-mode oscillation of a single flat-plate airfoil. The airfoil that generates these unsteady pressure distributions is constructed from a 0.038-cm- (0.015-in.-) thick sheet of stainless steel. The oscillating airfoil and mounting configuration shown in Fig. 3 are designed to maximize the amplitude and two dimensionality of the airfoil chordwise bending-mode shape. The airfoil is designed to resonate in a two-dimensional chordwise bending mode when sinusoidally excited at a frequency of 66 Hz. Chordwise bending oscillations are excited by a set of four surface-bonded piezoceramic motor elements. The piezoelectric actuators used to drive the airfoil measure 3.81 × 6.35 × 0.019 cm (1.5 × 2.5 × 0.0075 in.) and are formed from lead zirconate titanate (PZT) G-1195 piezoceramic material, chosen for its high piezoelectric–mechanical coupling effectiveness.

The mounting locations of the piezoelectric actuators on the airfoil surface are selected to maximize energy transfer from the crystals to the airfoil substructure while providing preferential excitation of the chordwise bending mode of oscillation. The recent work of Crawley and de Luis[4] suggests that piezoelectric actuators that locally strain the substructure should be located in regions of high average surface strain for the mode being excited. The region of maximum surface strain for the chordwise bending mode shape occurs between the chordal node lines and near airfoil midchord. Dimitriadis et al.[5] have shown that surface mounted actuators tend to excite plate modes having node lines near actuator boundaries. The actuators for the chordwise bending oscillating airfoil are located near the center of the airfoil with actuator edges lying along the two chordal node lines. Placement of the actuators in these locations promotes efficient excitation of the chordwise bending mode while minimizing the excitation of other plate modes. The chordwise bending oscillating airfoil is excited by applying a 66 Hz sinusoidally varying high-voltage signal to the piezoelectric actuators. The signal is supplied by a function generator and amplified to the required level using an audio amplifier and 3-to-1 step-up transformer.

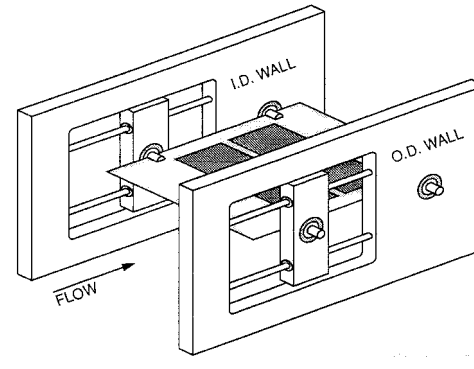

Fig. 3 Chordwise bending oscillating airfoil mounting configuration.

Data Acquisition and Analysis

Oscillating Airfoil Motion

Oscillating airfoil motion is monitored through measurement of the rotational oscillation of the airfoil mounting shafts. The leading- and trailing-edge shafts of the oscillating airfoil are affixed with linear taper precision potentiometers. Output of front and rear airfoil shaft potentiometer circuits are calibrated against airfoil leading- and trailing-edge midspan surface deflection measurements made using an Omron model 3Z4M Laser Displacement Sensor. Shaft potentiometer circuit calibrations are performed in a calibration wind tunnel at freestream velocities of 38.5, 25.5, and 19.1 m/s (121, 80.6, and 60.5 ft/

s), corresponding to reduced frequencies of $k = 2$, 3, and 4, respectively.

The oscillating airfoil mode shape is determined by measuring the airfoil surface displacement at points on a 5×11 point rectangular grid with surface displacement data acquired at a sampling rate of 1000 Hz in 2-s bursts. The airfoil surface displacement time traces are Fourier transformed to obtain displacement magnitude and phase information at each grid point. Airfoil motion is primarily contained within the first harmonic with higher harmonic magnitudes always less than 10% of the first harmonic. First harmonic phase information is used to determine mode shape node line locations. The chordwise bending-mode shape is characterized by the normalized first harmonic midspan cross section of the airfoil surface displacement $h(x)$, with the periodic airfoil motion described by

$$Y(x, t) = \mathrm{Re}[A_c h(x) e^{i\omega t}] \tag{3}$$

where A_c is the midspan leading-edge surface displacement defined positive leading-edge upward.

Figure 4 presents typical normalized first harmonic mode-shape data in the form of an airfoil surface contour plot. The nearly straight chordal contour lines indicate that the airfoil oscillates in a two-dimensional mode. The mode exhibits two chordal node lines at the airfoil shaft locations of 20 and 80% chord identified as bold contours in Fig. 4. Also shown are the midspan cross-sectional mode-shape data for the chordwise bending airfoil oscillating at reduced frequencies of $k = 2$, 3, and 4. Although the airfoil mode shape exhibits a slight dependence on the reduced frequency, the motion of the airfoil is characterized by a single normalized mode-shape curve $h(x)$, obtained by fitting the three mode-shape data sets with a sixth-order polynomial using the least-squares method.

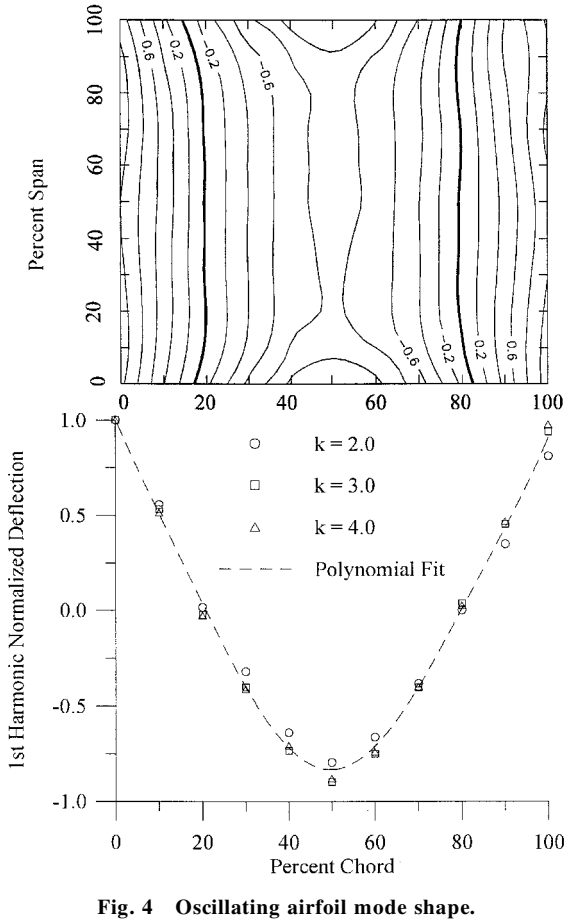

Fig. 4 Oscillating airfoil mode shape.

Unsteady Airfoil Surface Pressures

The magnitude and phase of the unsteady airfoil surface pressures induced by the chordwise bending-mode oscillation of a single airfoil in the annular airfoil cascade are measured using PCB (picocoulomb) Piezotronics model 103A piezoelectric dynamic pressure transducers. Transducer signals are amplified to required levels using a 12-channel instrumentation amplifier and power supply.

Unsteady pressure measurements are made at nine chordwise locations (2.5, 10.7, 23.2, 35.7, 50.0, 64.3, 76.5, 89.3, and 97.5% chord) on the chordwise bending oscillating airfoil surface. The elastic deformation of the airfoil associated with this mode of oscillation restricts the method in which surface pressure measurements can be made. The nine PCB dynamic pressure transducers are mounted external to the chordwise bending oscillating airfoil and connected to the airfoil surface midspan static pressure taps by sensing lines affixed to the lower surface of the airfoil. This transducer configuration is chosen because the mass of the transducers mounted on the airfoil surface would represent a significant percentage of the airfoil mass and would distort the airfoil chordwise bending mode shape. Mounting the transducers in the stationary frame also eliminates problems associated with subjecting the transducers to plate surface accelerations that can reach values of up to 32 g.

Dynamic pressure sensing line systems are known to exhibit nonlinear response in the frequency domain and must therefore be calibrated to correct for passage effects. Hoyniak and Fleeter[6] have shown that dynamic pressure transducer sensing lines can be calibrated for accurate measurement of unsteady pressures having frequencies that are well below the natural frequency of the sensing system. Dynamic calibration of the chordwise bending oscillating airfoil pressure sensing lines is performed in a resonator tube in a manner similar to that used by Henderson.[7] Calibration of the oscillating airfoil pressure sensing lines shows the frequency of interest, 66 Hz, to be well below the natural frequency of the sensing system that is approximately 350 Hz. Unsteady pressures having a fundamental frequency of 66 Hz can, therefore, be accurately measured through the transducer sensing line systems. For pressure measurements made on the surface of the stationary airfoils, the nine PCB dynamic pressure transducers are mounted inside the rigid airfoil and are also calibrated using the resonator tube facility.

Unsteady Aerodynamic Influence Coefficients

The unsteady surface pressures induced by the oscillating airfoil on itself and its stationary neighbors are measured in the Purdue Annular Cascade at freestream velocities corresponding to reduced frequencies of $k = 2$, 3, and 4 with the oscillating airfoil driven in the chordwise bending mode at 66 Hz. First, the self-induced unsteady aerodynamics are determined from unsteady surface pressure measurements on the surface of the oscillating airfoil. Data from the leading- and trailing-edge airfoil shaft potentiometer circuits and the pressure transducers are acquired at a sampling rate of 5000 Hz. One hundred bursts of 5000 samples of data are acquired from each transducer representing 66 chordwise bending airfoil oscillation cycles.

Next, the unsteady pressures on the stationary airfoils generated by the oscillating airfoil are measured. Unsteady surface pressure data are obtained for both upper and lower surfaces of the stationary airfoil while locating the oscillating airfoil in relative positions $n = 1$, 2, 3, and 4 as defined in Fig. 1. Unsteady surface pressures on the reference airfoil with the oscillating airfoil in all positions where $n \geq 4$ are found to be within the noise band of the dynamic pressure transducers and influence coefficients induced by the oscillating airfoil in these positions are therefore neglected.

The cascade is configured at zero stagger and is geometrically symmetric with respect to the reference airfoil. Thus,

unsteady surface pressure distributions are assumed to be symmetric and data are acquired on only one surface of the oscillating airfoil and are not acquired with the oscillating airfoil positioned at $n = -2$ and -3. However, the symmetry assumption is verified by acquiring data with the oscillating airfoil in the $n = -1$ position at a reduced frequency of $k = 3$.

The 100 bursts of airfoil surface pressure data acquired at each transducer location are ensemble averaged to eliminate pressure fluctuations not phase-locked to the oscillating airfoil motion. The representative unsteady pressure signal resulting from this averaging technique is then Fourier transformed to obtain unsteady airfoil surface pressure magnitude and phase information. The chosen acquisition sampling rate and duration provide a 1.0-Hz Fourier transform frequency resolution. First harmonic pressure signal magnitudes and phases are extracted from the transformed signals and adjusted to account for passage effects. Airfoil motion magnitude and phase are determined by averaging, transforming, and scaling the oscillating airfoil leading-edge potentiometer circuit signal in a manner identical to that described previously for the pressure signals. Finally, first harmonic airfoil surface pressures are referenced to the airfoil motion by subtracting the phase of the airfoil motion signal from each corresponding airfoil surface pressure phase.

The complex-valued unsteady aerodynamic pressure and pressure-difference influence coefficient are

$$\hat{C}^n_p(x) = \frac{p_1(x)}{\rho_0 U^2 (A_c/C)} \tag{4}$$

$$\Delta\hat{C}^n_p = \hat{C}^n_{pu} - \hat{C}^n_{pl} \tag{5}$$

where $p_1(x)$ is the complex-valued first harmonic of the airfoil static surface pressure.

The unsteady aerodynamics of a cascade having all airfoils oscillating at specified interblade phase angles are determined through a vector summation of the unsteady aerodynamic influence coefficients, per Eq. (1), with summation limits from $n = -3$ to 3.

Unsteady Aerodynamic Work per Cycle

The flutter stability of an oscillating airfoil cascade is quantified by the unsteady aerodynamic work done by the flowfield on a typical cascade airfoil through one cycle of airfoil motion. The work per cycle done on an airfoil undergoing arbitrary harmonic oscillation was derived by Verdon[8]

$$W_c = -\frac{C}{\omega}\int_0^{2\pi}\oint_{\mathcal{B}} \tilde{P}_{\mathcal{B}}(x, t)\left[\frac{\partial \boldsymbol{R}(x, t)}{\partial t}\cdot \hat{n}_{\mathcal{B}}\right] \mathrm{d}x\ \mathrm{d}(\omega t) \tag{6}$$

where the instantaneous airfoil surface pressure is defined

$$\tilde{P}_{\mathcal{B}}(x, t) = P_B(x) + \tilde{p}_{1\mathcal{B}}(x, t) + \cdots \tag{7}$$

with $P_B(x)$ the steady pressure at the mean airfoil surface and $\tilde{p}_{1\mathcal{B}}(x, t)$ the first harmonic unsteady pressure acting at the moving airfoil surface. The resulting nondimensional unsteady aerodynamic work per cycle or unsteady aerodynamic work coefficient expression for a flat-plate airfoil at zero mean incidence undergoing chordwise bending oscillations is

$$\bar{W}_c = \frac{W_c}{\rho_0 U^2 A_c^2} = -\pi\int_0^1 \mathrm{Im}[\Delta C_p(x)h(x)]\ \mathrm{d}x \tag{8}$$

where the cascade is classified as stable, neutrally stable, or unstable, depending upon whether $\bar{W}_c$ is less than, equal to, or greater than zero, respectively.

The unsteady aerodynamic work coefficient is a global measure of the stability of an oscillating cascade. A better understanding of stability is, however, gained by examining the distribution of work per cycle over the airfoil surface, thereby revealing intervals on the airfoil surface where local unsteady loads act to enhance or resist airfoil oscillation. The distribution of work per cycle over the airfoil surface, described by Verdon[8] as the pressure-displacement function, is represented here by the integrand of Eq. (8)

$$\bar{w}_c = -\pi\ \mathrm{Im}[\Delta C_p(x)h(x)] \tag{9}$$

and is termed the pressure-difference displacement function.

Experimental Results and Discussion

The chordwise bending unsteady aerodynamics of an annular cascade of flat-plate airfoils operating at zero mean incidence are experimentally investigated through measurement of the cascade unsteady aerodynamic influence coefficients. Experimental data are obtained at reduced frequencies of $k = 2$, 3, and 4 with corresponding cascade inlet Mach numbers of $M = 0.11$, 0.07, and 0.05. All data are obtained with the chordwise bending airfoil oscillating with a midspan leading-edge surface displacement amplitude A_c of approximately 0.18 cm (0.07 in.). The data are first presented in the form of unsteady surface pressure-difference influence coefficients. The influence coefficient data are then summed vectorially to determine the airfoil unsteady surface pressure-difference distributions for a cascade having all airfoils oscillating at interblade phase angles of $\beta = 0$ and 90 deg. Finally, these airfoil unsteady loading distributions are integrated to predict cascade stability through examination of the unsteady aerodynamic work per cycle of airfoil motion.

Experimental data are correlated with predictions obtained from LINSUB.[9] This model solves the inviscid subsonic linearized equations of continuity and momentum for a two-dimensional cascade of oscillating thin flat-plate airfoils. To predict chordwise bending-mode unsteady aerodynamics, the existing boundary conditions in LINSUB are modified. The airfoil surface flow tangency boundary condition is enforced by equating the normal flow velocity on the airfoil surface to the velocity of the moving airfoil surface. The nondimensional velocity normal to the airfoil surface, the upwash, for an arbitrary harmonic airfoil motion $y = \bar{y}(x)e^{i\omega t}$ is

$$\frac{\bar{w}(x)}{U} = \frac{\partial \bar{y}(x)}{\partial x} + ik\bar{y}(x) \tag{10}$$

where $\bar{y}(x)$ and $\bar{w}(x)$ are the airfoil oscillation and upwash oscillation amplitude distributions, respectively. Chordwise bending-mode oscillation is specified by defining the airfoil oscillation amplitude distribution as

$$\bar{y}(x) = (A_c/C)h(x) \tag{11}$$

Unsteady Aerodynamic Influence Coefficients

The experimentally measured airfoil surface chordwise bending unsteady pressure data are presented in the form of first harmonic unsteady pressure difference influence coefficients. Specifically, chordwise distributions of the pressure-difference influence coefficient on the instrumented reference airfoil located at position $n = 0$ in Fig. 1 are presented, for the oscillating airfoil located in the five relative positions defined by $n = -1$ through $n = 3$.

The experimentally determined chordwise bending coefficients $\Delta\hat{C}^n_p(x)$ are presented in Figs. 5 and 6 for the position $n = 0$ or reference airfoil, with the oscillating airfoil located at relative positions $n = 0$ and $n = 1$ at reduced frequencies of $k = 2$, 3, and 4. The 99% confidence uncertainties in the measured influence coefficient magnitude and phase are $\pm 8\%$ and ± 6 deg, respectively. LINSUB predictions resulting from the oscillation of a single airfoil at relative position n are also

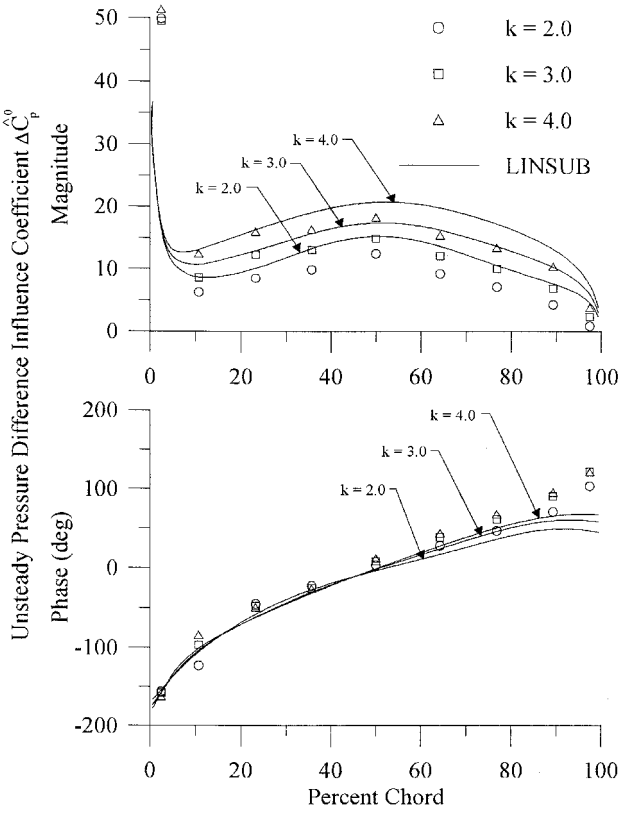

Fig. 5 Unsteady pressure-difference influence coefficient distributions, oscillating airfoil at relative position 0.

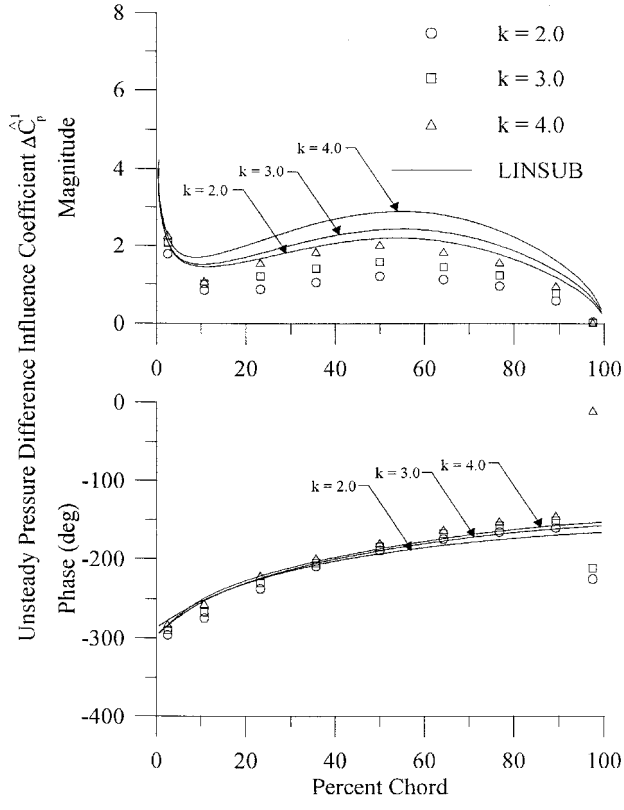

Fig. 6 Unsteady pressure-difference influence coefficient distributions, oscillating airfoil at relative position 1.

presented. These predictions are obtained by integrating the unsteady airfoil surface loadings calculated by LINSUB over all interblade phase angles, per Eq. (2).

The self-induced $\Delta\hat{C}_p^0(x)$ are shown in Fig. 5. The self-induced unsteady pressure difference magnitudes attain a maximum near the airfoil leading edge and fall off rapidly to a local minimum at approximately 10% chord for each value of the reduced frequency. Aft of 10% chord, the data increase to a local maximum near 50% chord and then fall to near zero at the airfoil trailing edge. The self-induced unsteady pressure-difference phase distributions are nearly linear with airfoil chord, lagging the airfoil motion over the forward half of the airfoil while leading the motion over the aft half of the airfoil. The self-induced unsteady pressure differences are in-phase with the airfoil motion near midchord and approximately out-of-phase with the airfoil motion at the leading edge. Also, the influence coefficient magnitudes increase with increasing reduced frequency with only minimal reduced frequency effect on the phase of the unsteady aerodynamic influence coefficients.

The influence coefficient distributions $\Delta\hat{C}_p^1(x)$ resulting from the oscillation of an airfoil at relative position $n = 1$ are shown in Fig. 6. The unsteady pressure-difference magnitudes exhibit the same trend as that found for the self-induced unsteady pressure differences at all reduced frequencies. The airfoil unsteady surface pressure differences lag the airfoil motion over the entire airfoil surface with the phase lag decreasing nearly linearly from leading to trailing edge. The unsteady pressure difference is approximately out-of-phase with the airfoil motion at midchord. The phase of the unsteady pressure measured at the airfoil trailing-edge pressure tap differs considerably from that expected at this chordwise location when following the trend exhibited by the experimental data. This discrepancy is attributed to difficulty in measuring the phase of a harmonic signal having an extremely small amplitude like the unsteady pressure at the trailing edge of the instrumented airfoil.

The influence coefficient distributions $\Delta\hat{C}_p^2(x)$ and $\Delta\hat{C}_p^3(x)$ are not presented, but exhibit trends similar to those found for $\Delta\hat{C}_p^1(x)$.

With regard to the data–theory correlation, the linearized unsteady cascade analysis accurately predicts the trends in both the unsteady pressure-difference magnitude and phase. However, the analysis overpredicts the unsteady pressure-difference influence coefficient magnitudes in all cases, with the exception of the near leading-edge pressure tap in the self-induced case (Fig. 5), where the pressure difference is significantly underpredicted. The phase of the unsteady pressure-difference influence coefficients is accurately predicted over all but the trailing-edge region where the prediction is slightly less than that measured experimentally. The analysis accurately predicts the trend of increasing influence coefficient magnitude with increasing reduced frequency. The minimal effect of reduced frequency on the phase of the unsteady pressure-difference influence coefficients is also accurately predicted by the linearized analysis.

Relative Position of Oscillating Airfoil

The effect of the oscillating airfoil relative position is shown in Fig. 7 with the first harmonic unsteady pressure-difference influence coefficients for the five relative positions, $n = -1$ through $n = 3$, of the oscillating airfoil superimposed at a reduced frequency of $k = 3$. The influence coefficient magnitude data are plotted on a logarithmic scale for ease of comparison. As previously noted, the influence coefficient magnitude distributions exhibit the same trend with the oscillating airfoil in each of the five relative positions. As expected, the magnitude of the unsteady pressure-difference influence coefficients decreases by approximately one order of magnitude each time the distance between the oscillating airfoil and the instrumented airfoil is increased by one blade spacing. This corresponds to an exponential decay of the pressure wave generated by the oscillating airfoil as it propagates away from the source.

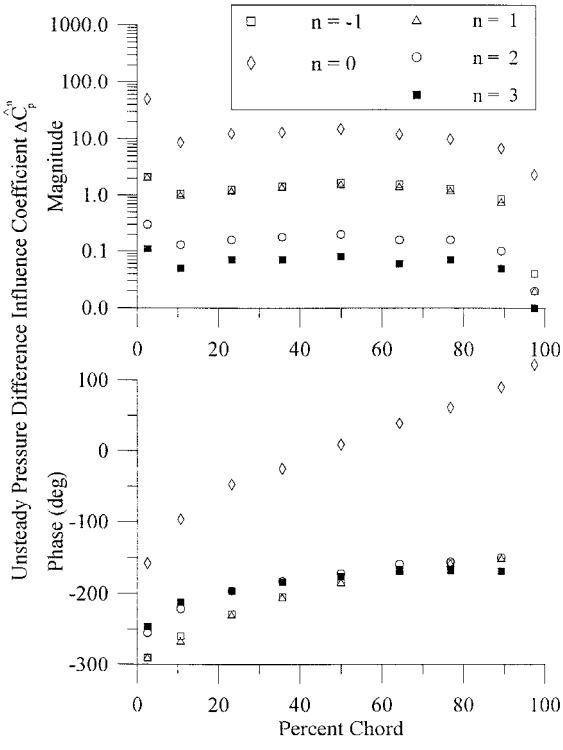

Fig. 7 Unsteady pressure-difference influence coefficient distributions, oscillating airfoil at relative position *n*, *k* = 3.0.

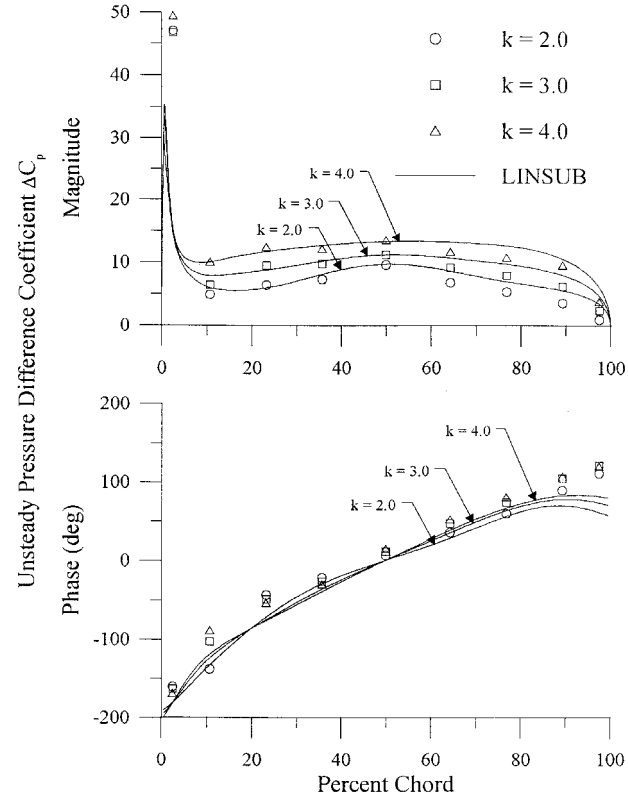

Fig. 8 Unsteady pressure-difference coefficient distributions β = 0.

The primary effect of the oscillating airfoil relative position on the influence coefficient phase is a difference between the self-induced or $n = 0$ airfoil surface pressure-difference phase distribution and the surface pressure-difference phase distributions induced on the reference airfoil by the oscillation of the $n = 1$ through $n = 3$ airfoils. The unsteady pressure differences induced by oscillation of the $n = 1$ through $n = 3$ airfoils lag the self-induced unsteady pressure differences by approximately 180 deg at the airfoil leading edge. This phase lag increases with increasing distance from the leading edge and reaches approximately 270 deg at the trailing edge of the airfoil. The phase of unsteady pressure differences induced on the $n = 0$ reference airfoil by the oscillation of airfoils in relative positions $n = 1$ through $n = 3$ are nearly identical.

The symmetry of the cascade with respect to the reference airfoil is also verified by the influence coefficient distributions shown in Fig. 7. The experimental influence coefficient data for oscillating airfoil in the $n = 1$ and -1 relative positions are identical to within experimental error, and thus, clearly validate the cascade symmetry assumption.

Airfoil Unsteady Aerodynamic Loading

The unsteady pressure-difference coefficient distributions obtained from a vector summation of the experimentally determined unsteady pressure-difference influence coefficients are presented in Figs. 8 and 9 for interblade phase angles of $\beta = 0$ and 90 deg, respectively. Also presented are the predictions obtained for an infinite cascade of simultaneously oscillating airfoils. The uncertainties in the experimental loading distributions are identical to those in the influence coefficient data.

At an angle of $\beta = 0$, all airfoils oscillate in-phase and the cascade operates in a superresonant mode, i.e., waves propagate away from the oscillating blade row unattenuated. As expected, the loading distributions follow the same trend exhibited by the self-induced influence coefficient distributions. The self-induced unsteady aerodynamics dominate the influence coefficient summation because the influence coefficients decrease exponentially with increasing distance between the instrumented and oscillating airfoils.

With the exception of a significant underprediction of the near leading-edge unsteady load magnitude, the linearized analysis predictions correlate well with the experimental influence coefficient summation airfoil loading distributions. The linearized analysis predicts the airfoil unsteady pressure magnitudes very well between 10–50% chord, while slightly overpredicting the unsteady loading magnitude over the aft portion of the airfoil. The best phase data–theory correlation occurs between 35–75% chord. The phase of the unsteady airfoil loading is underpredicted in the airfoil leading- and trailing-edge regions. As was the case with the influence coefficient data, the variations of data and prediction with reduced frequency are in good agreement, with the analysis correctly predicting the observed trend of increased unsteady loading with increasing reduced frequency.

A cascade oscillating at an interblade phase angle of $\beta = 90$ deg (Fig. 9), operates in a subresonant mode, i.e., waves decay exponentially with increasing distance from the oscillating blade row. As in the superresonant case, the trends in the unsteady pressure difference loading magnitude and phase distributions follow those observed for the self-induced influence coefficients distributions.

Agreement between the experimental data and linearized analysis prediction of the subresonant mode loadings is not as good as in the superresonant case. The linearized analysis overpredicts the unsteady pressure-difference coefficient magnitudes on the airfoil surface aft of 10% chord. As in the superresonant case, the unsteady pressure-difference magnitudes in the airfoil near leading-edge region are significantly underpredicted.

Cascade Flutter Stability and Unsteady Aerodynamic Work per Cycle

The susceptibility of the oscillating cascade to chordwise bending flutter is quantified by the aerodynamic work done by the flowfield on a typical oscillating airfoil over one cycle of airfoil motion. This unsteady aerodynamic work is a direct

measure of the energy transfer from the flowfield to the oscillating airfoil. Conversely, the unsteady aerodynamic work per cycle is a measure of the cascade aerodynamic damping or the ability of the cascade to dissipate energy fed into the cascade by the unsteady flowfield.

A typical flutter stability plot for the chordwise bending oscillating cascade is presented in Fig. 10. The unsteady aerodynamic work per cycle coefficient is plotted as a function of interblade phase angle for the cascade operating at a reduced frequency of $k = 3$. The corresponding linearized analysis prediction is also presented.

The consistently positive values of the experimentally determined aerodynamic work per cycle coefficient over the entire range of interblade phase angle indicate that the cascade is always unstable. The cascade aerodynamic work per cycle coefficient is minimum at $\beta = 0$ and increases to a maximum at $\beta = \pm 180$ deg. This indicates that this cascade configuration provides maximum aerodynamic damping of the chordwise bending mode for in-phase cascade airfoil oscillations and minimum aerodynamic damping when the cascade airfoils oscillate out-of-phase. The aerodynamic work per cycle is symmetric with respect to $\beta = 0$ as a result of the cascade symmetry with respect to the $n = 0$ reference airfoil.

The data and prediction show good trendwise agreement. Both the data and prediction show the cascade aerodynamic work per cycle coefficient to be a minimum at $\beta = 0$, increasing with increasing β until reaching $\beta = 100$ deg. For values of interblade phase angle between 100 and 180 deg, the experimentally determined values of aerodynamic work per cycle coefficient continue to increase, while the predicted values decrease slightly as β increases to 180 deg. However, the linearized analysis prediction of cascade stability correlates poorly with the data. The stability prediction for the chordwise bending oscillating cascade is symmetric with respect to $\beta = 0$ deg, indicating stability for $|\beta| < 40$ deg and only marginal instability for all other values of interblade phase angle. Also, the aerodynamic work per cycle prediction exhibits discontinuities at resonant values of the interblade phase angle. These discontinuities are a result of mathematical singularities in the linearized unsteady flow equations at acoustic resonances. The absence of discontinuities in the experimental data is attributable to the data being acquired in the form of influence coefficients by oscillating a single airfoil in the cascade. As a result, the acoustic resonance condition in which acoustic energy propagates along the blade row is not physically encountered.

The large discrepancy between the experimentally determined and analytically predicted cascade stability is explained through examination of the chordwise distribution of work per cycle along the airfoil surface, i.e., the unsteady pressure-difference displacement function. Figure 11 presents the experimentally determined unsteady pressure-difference displacement function distribution and corresponding prediction for a reduced frequency of $k = 3$ and an interblade phase angle of $\beta = 90$ deg. The trends exhibited by these data are typical of all interblade phase angles. The data and prediction correlate moderately well with the exception of the airfoil leading-edge region near the 2.5% chord pressure tap where the difference between the measured and predicted unsteady pressure-difference displacement function is very large. Aft of 10% chord, there is good data-prediction trendwise agreement of the unsteady pressure-difference displacement function, although the experimental data are underpredicted between 35–65% chord and aft of 85% chord.

The local transfer of energy between the oscillating airfoil and the flowfield is quantified by the unsteady pressure-differ-

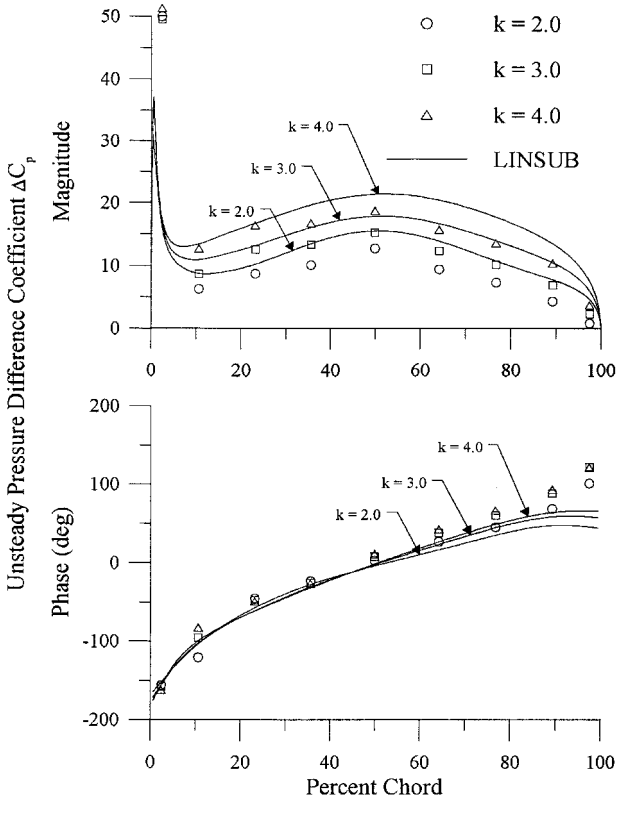

Fig. 9 Unsteady pressure-difference coefficient distributions $\beta = 90$.

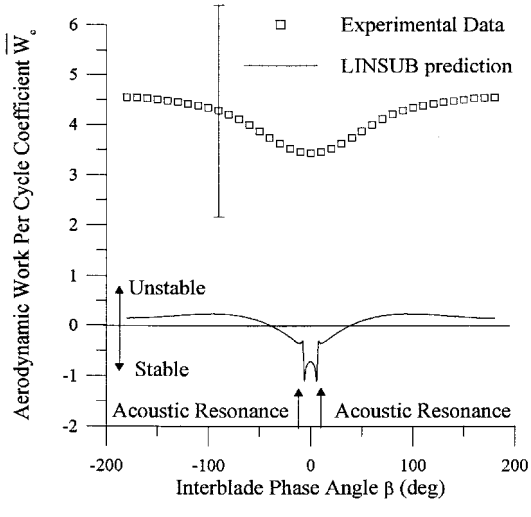

Fig. 10 Unsteady aerodynamic work per cycle coefficients $k = 3.0$.

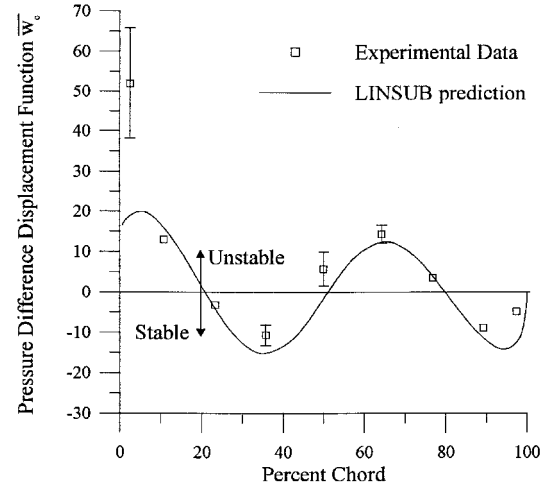

Fig. 11 Pressure-difference displacement function distribution $k = 3.0$ and $\beta = 90$.

ence displacement function. The chordwise aerodynamic work distribution of Fig. 11 shows that between 20–50% chord and aft of 80% chord, energy is transferred locally from the oscillating airfoil to the flowfield. This energy transfer indicates aerodynamic damping of chordwise bending airfoil oscillations through suppression of airfoil motion by local surface unsteady pressure forces. Between 0–20% chord and between 50–80% chord, energy is transferred locally from the flowfield to the airfoil, thereby enhancing the chordwise bending airfoil oscillations.

The largest discrepancy between the data and the predicted unsteady pressure-difference displacement function occurs in the leading-edge region. The prediction and the data compare favorably at the 10.7% chord pressure tap location, showing a difference of less than 20%. However, a 65% difference is observed at the 2.5% chord pressure tap location. The large discrepancy between the experimentally determined and the predicted stability curves of Fig. 10 is attributed primarily to the behavior of the pressure displacement function at this 2.5% chord position.

In the airfoil trailing-edge region, negative values of the unsteady pressure-difference displacement function are predicted. The predicted function has a value of zero at 80 and 100% chord, and reaches a local minimum at approximately 95% chord. Only two experimental data points are obtained on this region of the airfoil surface. These data are underpredicted by the linearized analysis. In addition, because the experimental data are integrated numerically using the trapezoid rule, the absence of a third experimental data point between 89.3 and 97.5% chord where a local minimum is expected results in a significant discrepancy between the integration of the experimental data and the prediction.

The predicted distribution of unsteady work along the oscillating airfoil surface between the airfoil chordal node lines, 20–80% chord, suggests that the net transfer of energy from the flowfield to the oscillating airfoil in this region is approximately zero. However, the experimental data indicate that the unsteady loading on the central region of the airfoil surface produces a net destabilizing effect on chordwise bending airfoil oscillation. The discrepancy between measured and predicted contributions to stability is also attributed, in part, to the underprediction of the pressure-difference displacement function at 35.7 and 50% chord.

Further insight into the discrepancy between the measured and predicted cascade stability results is gained through an uncertainty analysis of the data. Uncertainties in the measured unsteady pressures and displacements are propagated through the pressure-difference displacement function and stability equations to quantify the uncertainty in the experimentally determined cascade stability data. The effect of uncertainty in the measured unsteady loading on the unsteady pressure-difference displacement function is investigated by rewriting Eq. (9) as

$$\bar{w}_c = -\pi |\Delta C_p| \sin(\phi_p) h(x) \tag{12}$$

where $|\Delta C_p|$ and ϕ_p are the magnitude and phase of the unsteady pressure-difference coefficient, respectively.

Applying the uncertainty analysis methods of Kline and McClintock[10] to Eq. (12) neglecting the uncertainty in the measured mode-shape distribution $h(x)$, the percent uncertainty in the calculated pressure-difference displacement function is

$$\sigma_{\bar{w}_c}/\bar{w}_c = \sqrt{(\sigma_{\Delta C_p}/|\Delta C_p|)^2 + (\sigma_{\phi_p}/\tan\phi_p)^2} \tag{13}$$

where the σ represent the uncertainty intervals for the measured and calculated quantities.

The uncertainty in the pressure-difference displacement function is inversely proportional to the tangent of the unsteady pressure-difference phase. Thus, large uncertainties are expected where the phase of the unsteady pressure acting on the airfoil surface is near 0 and 180 deg.

Uncertainties in the pressure-difference displacement function distribution (Fig. 11) are shown on each data point as error bars that represent a 99% confidence interval. Omitted error bars indicate that the confidence interval falls within the symbol. Re-examination of the experimentally determined airfoil unsteady aerodynamic loading distribution presented in Fig. 9 reveals that the unsteady pressure difference at 2.5% chord on the surface of the chordwise bending oscillating airfoil has large magnitude and is approximately out-of-phase with the airfoil motion. Consequently, the pressure-difference displacement function is highly sensitive to variations in the phase of the unsteady pressure there, shown by the large uncertainty interval indicated in Fig. 11 at this chordwise location. In the midchord region, the unsteady airfoil surface pressure is approximately in-phase with airfoil chordwise bending oscillations, resulting in relatively large uncertainties in the pressure-difference displacement function at the 35.7, 50, and 64.3% pressure tap locations. The chordwise locations of large uncertainties in the pressure-difference displacement function thus correspond to regions on the airfoil surface where discrepancies between the measured and predicted functions show disagreement.

Uncertainty in the experimentally determined stability parameter, aerodynamic work per cycle, is determined through perturbation of the pressure-difference displacement function values prior to integration per Eq. (8). Uncertainty in the aerodynamic work per cycle is indicated in Fig. 10 as a single 99% confidence error bar that represents the uncertainty over the entire curve. The indicated uncertainty of approximately $\pm 50\%$ is primarily because of the sensitivity of the pressure-difference displacement function to uncertainties in measured unsteady pressure phase in the midchord and leading-edge regions of the airfoil surface.

The origin of the large discrepancy between the experimentally determined cascade chordwise bending stability and the prediction can now be attributed to three factors. The primary cause for the discrepancy between the experimental and predicted cascade stability parameter is the 65% difference in the measured and predicted unsteady pressure-difference magnitude at the 2.5% chord pressure tap location. A second cause for the difference in measured and predicted cascade stability is the sensitivity of the pressure-difference displacement function to variations in the phase of the measured airfoil unsteady surface pressure in the leading edge and midchord regions. Small uncertainties in unsteady pressure phase are shown to lead to large uncertainties in pressure-difference displacement function in these regions. Finally, the stability of an oscillating cascade is described by the aerodynamic work per cycle coefficient, determined by chordwise integration of the unsteady pressure-difference displacement function. As shown in Fig. 11, a chordwise distribution of the unsteady pressure-difference displacement function for an airfoil oscillating in chordwise bending is an irregular curve that oscillates about zero and has four chordwise relative extrema. Accurate numerical integration of this irregular curve is difficult with only a relatively small number of data points along the airfoil chord. If a relative maximum or minimum of the unsteady pressure-difference displacement function lies between two data points, as in the trailing-edge region of the experimental chordwise bending data, large errors in the calculation of the aerodynamic work per cycle coefficient may result.

Summary and Conclusions

The chordwise bending unsteady aerodynamics of an annular cascade of flat-plate airfoils are investigated utilizing an experimental influence coefficient technique. A single airfoil in the cascade is forced to oscillate in a chordwise bending mode over a range of reduced frequencies. Unsteady surface pressures induced on the oscillating airfoil and its stationary neighbors are measured to determine the unsteady aerodynamic influence coefficients. These influence coefficients are

then summed vectorially to obtain unsteady airfoil surface loadings. The experimental data are correlated with predictions from linearized unsteady aerodynamic theory.

The chordwise influence coefficient distribution data and linear theory predictions exhibit trendwise agreement. The measured and predicted trendwise effect of the reduced frequency on the chordwise bending cascade unsteady aerodynamics also exhibit good correlation. Both the data and predictions show an increase in the unsteady pressure-difference influence coefficient magnitudes with increasing reduced frequency and a minimal reduced frequency effect on the phase of the unsteady influence coefficients. However, the correlation of the experimentally determined and predicted influence coefficient magnitudes is not as good. At the airfoil leading-edge pressure tap location, 2.5% chord, the magnitude of the influence coefficients is severely underpredicted at all reduced frequencies. Aft of this leading-edge data point, the magnitude of the influence coefficient data is slightly overpredicted. Phase agreement between the experimental data and predictions is generally good.

The unsteady aerodynamic influence coefficient data are vectorially summed to determine the unsteady loading distributions for an equivalent cascade having all airfoils oscillating at a constant interblade phase angle. The agreement between experimental and predicted airfoil unsteady loading distributions is analogous to that found for the influence coefficient data, but exhibits dependence on the mode of cascade operation, being better when cascade waves are superresonant than when the cascade operates in the subresonant mode.

The susceptibility of the cascade configuration to chordwise bending mode flutter is quantified through the calculation of the aerodynamic work done by the flowfield on the oscillating cascade over one cycle of airfoil motion. The experimentally determined values of chordwise bending-mode aerodynamic damping and the corresponding predictions at all interblade phase angles are in good trendwise agreement. However, the experimentally determined values of the aerodynamic damping indicate that the cascade is unstable at each reduced frequency over the entire range of interblade phase angles while predictions of cascade stability indicate the cascade to be stable or only marginally unstable at all values of interblade phase angle. This discrepancy is attributed primarily to a large difference between measured and predicted unsteady loading magnitude near the leading edge of the airfoil and to the sensitivity of the pressure-difference displacement function to uncertainty in measured unsteady surface pressure phase in the midchord and leading-edge regions. Improvement in the agreement between the experimentally determined and predicted cascade stability may be achieved by increasing the number of pressure tap locations on the airfoil surface in the leading- and trailing-edge regions.

Acknowledgment

This research was supported, in part, by the U.S. Army Research Office. This support is gratefully acknowledged.

References

[1]Kovats, Z., "Predicting Aerodynamic Damping and Stability of Low-Pressure Turbine Blades Using the Influence Coefficient Method," *Proceedings of the ASME Cogen-Turbo Exposition, IGTI*, Vol. 6, 1991, pp. 251–262.

[2]Buffum, D. H., and Fleeter, S., "Aerodynamics of a Linear Oscillating Cascade," NASA TM 103250, Aug. 1990.

[3]Hanamura, Y., Tanaka, H., and Yamaguchi, K., "A Simplified Method to Measure Unsteady Forces Acting on the Vibrating Blades in Cascade," *Bulletin of the Japan Society of Mechanical Engineers*, Vol. 23, No. 180, 1980, pp. 880–887.

[4]Crawley, E. F., and De Luis, J., "Use of Piezoelectric Actuators as Elements of Intelligent Structures," *AIAA Journal*, Vol. 25, No. 10, 1987, pp. 1373–1385.

[5]Dimitriadis, E. K., Fuller, C. R., and Rogers, C. A., "Piezoelectric Actuators for Distributed Vibration Excitation of Thin Plates," *Journal of Vibration and Acoustics*, Vol. 113, Jan. 1991, pp. 100–107.

[6]Hoyniak, D., and Fleeter, S., "Frequency Response of Dynamic Pressure Transducer Sensing Line Configurations," 28th International Instrumentation Symposium, Instrumentation Society of America, March 1982.

[7]Henderson, G. H., "Forcing Function and Steady Loading Effects on Unsteady Aerodynamic Gust Response," Ph.D. Dissertation, Purdue Univ., West Lafayette, IN, 1991.

[8]Verdon, J. M., "The Unsteady Aerodynamic Response to Arbitrary Modes of Blade Motion," *Journal of Fluids and Structures*, Vol. 3, 1989, pp. 255–274.

[9]Smith, S. N., "Discrete Frequency Sound Generation in Axial Flow Turbomachines," Aeronautical Research Council, R & M 3709, Cambridge, England, UK, March 1972.

[10]Kline, S. J., and McClintock, F. A., "Describing Uncertainties in Single-Sample Experiments," *Mechanical Engineering*, Vol. 75, No. 1, 1953, pp. 3–8.